Cavity Optomechanics of Levitated Nanodumbbells: Nonequilibrium Phases and Self-Assembly

W. Lechner,[1,2,*] S. J. M. Habraken,[1,2] N. Kiesel,[3] M. Aspelmeyer,[3] and P. Zoller[1,2]

[1]*Institute for Quantum Optics and Quantum Information, Austrian Academy of Sciences, 6020 Innsbruck, Austria*
[2]*Institute for Theoretical Physics, University of Innsbruck, 6020 Innsbruck, Austria*
[3]*Vienna Center for Quantum Science and Technology (VCQ), Faculty of Physics, University of Vienna, Boltzmannagsse 5, 1090 Vienna, Austria*

(Received 17 January 2013; published 5 April 2013)

Levitated nanospheres in optical cavities open a novel route to study many-body systems out of solution and highly isolated from the environment. We show that properly tuned optical parameters allow for the study of the nonequilibrium dynamics of composite nanoparticles with nonisotropic optical friction. We find optically induced ordering and nematic transitions with nonequilibrium analogs to liquid crystal phases for ensembles of dimers.

DOI: 10.1103/PhysRevLett.110.143604 PACS numbers: 42.50.Wk, 07.10.Cm, 73.22.−f

Introduction.—The interaction between light and matter has been one of the central driving forces behind recent developments in condensed matter physics with nanoparticles [1]. Optical tweezers [2,3] and confocal microscopy [4] have made it possible to study many-body systems of nanoparticles in solutions in real time and with single-particle resolution [5–8]. Recently, it has been proposed to optically levitate and cool single nanospheres inside an optical cavity [9–12]. While in the realm of soft-matter physics, this may provide an alternative to confinement in a solution [13], from a quantum-optics point of view such a setup provides a versatile alternative to conventional optomechanical systems [14–16]. Combined with optomechanical cooling and trapping techniques of single particles, this may even open the possibility to study fundamental aspects of quantum mechanics with mesoscopic objects [11,17,18]. Here, we focus on the dynamics of many, interacting particles in the presence of optomechanical cooling. While many-body systems with nonuniform cooling have been studied with atoms and ions [19], the possibility to create complex structures with nanospheres offers completely new opportunities to study pattern formation and self-assembly. With novel synthesis methods it is now possible to design compound structures ranging from dimers to networks of nanospheres connected by springlike biomolecules [20–26]. A distinctive feature of the self-assembly of composite particles is that the emerging patterns are characterized not only by their positions, but also by their individual orientations [27,28]. The nonequilibrium self-assembly of such nanostructures in the presence of nonisotropic optical cooling is an open question, and holds the promise of a new means to optical control of pattern formation and novel nonequilibrium liquid crystal phases.

In this Letter, we study the dynamics and self-assembly of levitated nanosphere dimers in the presence of optomechanical friction inside a two-mirror cavity. The particles are subject to thermal forces and coupled to a cavity mode which is driven by an external laser and damped by the cavity decay. The optomechanical interaction gives rise to an optical potential and a cooling force along the cavity axis. By compensating the potential with a second optical mode, the remaining optomechanical effect is friction along the cavity axis. Figure 1 illustrates the system we have in mind. The nanospheres are harmonically trapped and confined to the xy plane, where x is the cavity axis. We show that the steady-state orientation of a single dimer is nonuniform in the presence of optical friction. Remarkably, the full range of preferred orientations from 0 to $\pi/2$ is accessible by appropriately tuning the experimental parameters. In a many-body system, the presence of additional direct interactions between the individual nanospheres, leads to competition between the natural triangular ordering of a

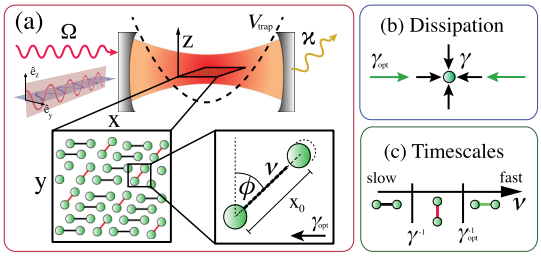

FIG. 1 (color online). (a) Levitated dimers composed of dielectric nanospheres in a laser driven optical two-mode cavity with laser strengths $\Omega_{1,2}$, a decay rate κ, and an additional harmonic trap V_{trap}. The orientation of the dimers is denoted ϕ, their equilibrium separation x_0, and their frequency ν. The direct pair interaction between the nanospheres leads to liquid crystal phases with rich dimer patterns. (b) The particles are in contact with a thermal bath with coupling γ. The cavity-particle interaction results in strong additional dissipation in one spatial direction only, which acts as an effective zero temperature bath γ_{opt}. (c) Comparison of the relevant time scales: We assume that γ_{opt} is faster than γ and find three qualitatively different regimes, which give rise to different orientations, depending on the relative timescales.

 © 2013 American Physical Society

two-dimensional crystal and dissipation-induced ordering. Compared to other approaches to dynamical ordering of dimers, such as shear [29] or static electric fields [30], this method offers additional advantages: (a) the orientation depends on the frequency of the vibrational mode of the dimers which allows for individual ordering in multispecies systems and (b) in addition to ordering at the level of single particles, nonuniform friction also leads to novel liquid crystal phases at the many-body level (see Fig. 3). We identify three relevant time scales in this system: the frequency of the vibrational mode of the dimers ν, the optomechanical damping rate γ_{opt}, and the rate of thermalization γ. For limiting cases we present analytic results on the ordering of individual dimers and numerical results on the nonequilibrium many-body dynamics.

Model.—We consider a system of $N/2$ dimers consisting of N nanospheres, trapped inside an optical cavity. The Hamiltonian is decomposed as $H = H_{\mathrm{sys}} + H_{\mathrm{om}}$ with

$$H_{\mathrm{sys}} = \sum_{i=1}^{N}\left(\frac{\mathbf{p}_i^2}{2m} + V_{\mathrm{trap}}(\mathbf{x}_i)\right) + \sum_{i=1}^{N/2}\frac{m\nu^2}{2}(|\mathbf{x}_{2i-1} - \mathbf{x}_{2i}| - x_0)^2 + \Gamma_0\sum_{i\neq j}V_{\mathrm{int}}(|\mathbf{x}_i - \mathbf{x}_j|), \quad (1)$$

the system Hamiltonian. Here, m is the mass of the nanospheres, $\mathbf{x}_j$ and $\mathbf{p}_j$ are the position and momentum of particle j, respectively, V_{trap} is the trapping potential, ν the frequency of the vibrational mode of the dimers, x_0 is the equilibrium separation and V_{int} is the direct dipolar pair interaction, which can be tuned by the parameter Γ_0 [6]. In a frame, rotating with the laser drive, the optomechanical Hamiltonian is given by

$$H_{\mathrm{om}} = -\Delta(\mathbf{x}_1 \ldots \mathbf{x}_N)|a|^2 + \Omega(a + a^*) + V_c, \quad (2)$$

where $a(t)$ $[\sqrt{Js}]$ is a normal variable, which describes the dynamics of the optical mode, Ω $[\sqrt{J/s}]$ characterizes the drive strength, V_c is a second compensating potential, and $\Delta = \omega_d - \omega(\mathbf{x}_1, \ldots, \mathbf{x}_N)$ is the detuning from the cavity resonance with ω_d the drive frequency. The interaction derives from the electric polarizability α_p of the nanospheres [9,10], which, for subwavelength particles, gives rise to a position-dependent cavity resonance frequency $\omega(\mathbf{x}_1, \ldots, \mathbf{x}_N) = \omega_0 - (gC/2)\sum_j|\mathbf{F}(\mathbf{x}_j)|^2$, where ω_0 is the bare cavity frequency. $\mathbf{F}(\mathbf{x})$ is the normalized mode function of the cavity mode, C is the mode volume, and $g = \alpha_p\omega_0 V/C$ is the optomechanical coupling strength, which is proportional to the volume of the particle V. We assume that the cavity mode can be approximated by a standing wave $\mathbf{F}(\mathbf{x}) \simeq \boldsymbol{\epsilon}\sqrt{2/C}\sin(kx)$, where k is the wave number and $\boldsymbol{\epsilon}$ is the polarization in the yz plane, so that $\Delta(\mathbf{x}_1, \ldots, \mathbf{x}_N) = \Delta(x_1, \ldots, x_N)$.

The full dynamics of the optical part, including decay from the cavity, is described by the equations of motion for the optical amplitude $\dot{a} = [i\Delta(x_1, \ldots, x_N) - \kappa]a + i\Omega$, where κ is the field decay rate. The drive can be eliminated by the transformation $a \to \alpha + a'$ with $\alpha = \Omega/(\bar{\Delta} + i\kappa)$ the average amplitude and $\bar{\Delta} = (\omega_d - \omega)$ the detuning from the bare cavity resonance. The equation of motion for the transformed optical amplitude is $\dot{a}' = (i\bar{\Delta} - \kappa)a' + i(\Delta(x_1, \ldots, x_N) - \bar{\Delta})(\alpha + a')$. Substitution of $a \to \alpha + a'$ in the first term in Eq. (2) gives rise to four terms. One of them corresponds to an effective optical potential along the cavity axis $V(x_1, \ldots, x_N) = -|\alpha|^2\Delta(x_1, \ldots, x_N)$, which can be compensated by V_c of the second optical mode. For the choice of a mode separated by one free spectral range from ω, the mode function in the focal range of the cavity is approximately given by $\mathbf{G}(x) \simeq \boldsymbol{\eta}\sqrt{2/C}\cos(kx)$, where $\boldsymbol{\eta}$ is the polarization. When $\boldsymbol{\epsilon}$ and $\boldsymbol{\eta}$ are orthogonal, the two modes do not interfere and the effective potentials add up, i.e., $V(x_j) = -g[|\alpha_1|^2\sin^2(kx_j) + |\alpha_2|^2\cos^2(kx_j)]$, where $\alpha_{1,2}$ are the amplitudes of the first and second mode, respectively. For $|\alpha_1| = |\alpha_2| = |\alpha|$, the potential is independent of x_j and the forces cancel. The second mode is driven on resonance and therefore does not lead to additional damping (or amplification).

We find the equations of motion of the nanosphere positions and momenta

$$\dot{\mathbf{x}}_i = \mathbf{p}_i/m,$$
$$\dot{\mathbf{p}}_i = -\frac{\partial H_{\mathrm{sys}}}{\partial \mathbf{x}_i} + (\alpha a'^* + \alpha^* a' + |a'|^2)\frac{\partial\Delta(x_1, \ldots, x_N)}{\partial x_i}. \quad (3)$$

The cavity decay rate κ sets a finite time scale for the cavity to respond to changes in the particle positions so that the optomechanical feedback does not only depend on the particle positions, but also on the particle momenta along the cavity axis [14]. This gives rise to amplification (for $\bar{\Delta} > 0$) or damping (for $\bar{\Delta} < 0$), respectively. Optomechanical cooling of nanospheres has been studied previously in the Lamb-Dicke regime [9], while here, we focus on a different regime, similar to Ref. [31], in which the particles move almost freely and the relevant frequency stems from the modulation of the optical feedback force at $\omega_{\mathrm{mod}} = 2kp/m$. The damping force has resonances for $\bar{\Delta} = \pm|\omega_{\mathrm{mod}}|$, while in the regime we are interested in, $|p| \ll m\bar{\Delta}/(2k)$, the cooling rate is approximately constant

$$\gamma_{\mathrm{opt}} \simeq \frac{2g^2|\alpha|^2k^2\bar{\Delta}\kappa}{m(\bar{\Delta}^2 + \kappa^2)^2}. \quad (4)$$

With an additional thermal force, the equations of motion take the form of modified Langevin equations (see Ref. [32]) with

$$m\ddot{x}_i = -\frac{\partial H_{\mathrm{sys}}}{\partial x_i} - m(\gamma + \gamma_{\mathrm{opt}})\dot{x}_i + \xi_{x_i},$$
$$m\ddot{y}_i = -\frac{\partial H_{\mathrm{sys}}}{\partial y_i} - m\gamma\dot{y}_i + \xi_{y_i}. \quad (5)$$

Here, $(x_i, y_i) = \mathbf{x}_i$ are the components of the position vector of particle i, γ is the rate of thermalization, and ξ_x and ξ_y are mutually uncorrelated Langevin forces, as characterized by $\langle \xi_{x,y}(t)\xi_{x,y}(t')\rangle = k_B T m\gamma\delta(t - t')$.

Results.—We first focus on the dynamics of a single dimer described by Eq. (5). Separating the dynamics into the trivial center-of-mass motion and the relative coordinates $(\mathbf{x}_1 - \mathbf{x}_2)/\sqrt{2} \equiv (x, y)$, and to the extent that optomechanical coupling between the particles can be neglected, the nonlinear force is $\frac{\partial H_{\rm sys}}{\partial \mathbf{r}} = -\mathbf{r}m\nu^2\{1 - [2x_0/(x^2 + y^2)]^{1/2}\}$, where $\mathbf{r} = (x, y)$ and x_0 is the dimer separation. Figures 2(a)–2(c) show the steady state solutions of the orientation of single dimers as a function of the dimer frequency for various cooling rates from numerical integration of Eq. (5). Remarkably, when exposed to unidirectional friction, a loosely connected dimer, as well as a rigid rotor, tends to align orthogonal to the direction of friction, whereas a dimer of moderate stiffness aligns parallel to it. This can be understood from three competing effects which derive from the order of the relevant time scales in the system (see Fig. 1(c)): γ^{-1}, $\gamma_{\rm opt}^{-1}$ and ν^{-1}. While γ and $\gamma_{\rm opt}$ set the scales of thermalization and nonuniform friction, ν sets the time scale at which the degrees of freedom mix due to the nonlinear nature of the force term. Assuming that $\gamma_{\rm opt} > \gamma$, there are

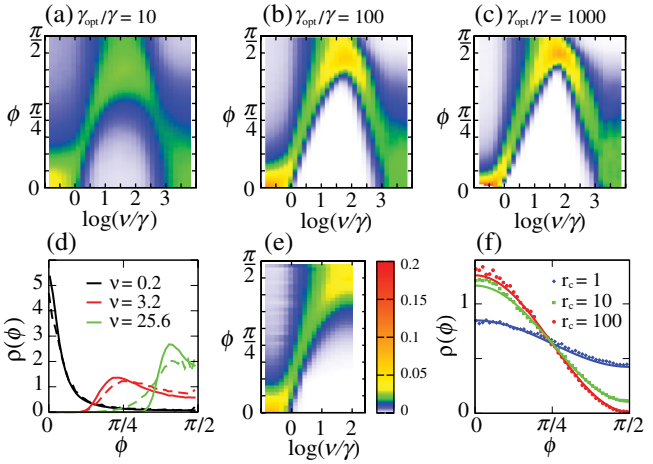

FIG. 2 (color online). Steady-state probabilities of the orientation ϕ as a function of the dimer frequency from numerical integration of the second order Langevin equations (5) for cooling rate ratios $\gamma_{\rm opt}/\gamma = 10$ (a), $\gamma_{\rm opt}/\gamma = 100$ (b), and $\gamma_{\rm opt}/\gamma = 1000$ (c). The comparison of the analytic expressions (6) for small frequencies [(d) dashed lines] and numerical results [(d) full lines] show good agreement over a wide range of frequencies. (e) Analytic results from Eq. (6) for a range of frequencies with $\gamma_{\rm opt}/\gamma = 100$ predicts the transition from $\phi = 0$ orientation to $\phi = \pi/2$. For larger frequencies the model breaks down as it predicts $\phi = \pi/2$ for large ν (e). In the rigid-rotor regime, the analytic approximation Eq. (8) is in agreement with the numerical simulation as shown for various cooling rates $r_c = \gamma_{\rm opt}/\gamma$ (f).

three limiting parameter regimes: (i) $\gamma_{\rm opt} \gg \gamma \gg \nu$, (ii) $\gamma_{\rm opt} \gg \nu \gg \gamma$, and (iii) $\nu \gg \gamma_{\rm opt} \gg \gamma$. In the following we analytically study these limiting cases and give an intuitive explanation of this remarkable nonequilibrium ordering phenomenon.

In (i) and (ii), $\gamma_{\rm opt}$ is the largest scale. Due to the resulting separation of time scales of the motion in the x and y directions, the steady-state distribution is of the form $P(x, y) = P(y|x)P(x)$. Here, $P(y|x)$ is the normalized steady-state distribution of the fast y direction given a fixed x. Consequently, the average energy $\langle V\rangle_x = \int_{-\infty}^{\infty} V(x, y)P(y|x)$ determines the distribution $P(x)$ for the x direction via a Markov process with the scaled temperature $T_x = T\gamma/(\gamma + \gamma_{\rm opt})$, thus

$$P(x, y) = \frac{e^{-V(x,y)/(k_B T)}}{\int_{-\infty}^{\infty} dy e^{-V(x,y)/(k_B T)}} \frac{e^{-\langle V\rangle_x/(k_B T_x)}}{\int_{-\infty}^{\infty} dx e^{-\langle V\rangle_x/(k_B T_x)}}. \quad (6)$$

In regime (i), the spatial fluctuations are much larger than x_0, so that $V(x, y) \simeq m\nu^2(x^2 + y^2)/2$ and the integrals can be evaluated analytically. The distribution $P(\phi) = \int_0^{\infty} rdrP(r\cos\phi, r\sin\phi)$ for the orientation of the dimer ϕ is found as

$$P(\phi) = \frac{\sqrt{\gamma(\gamma + \gamma_{\rm opt})}}{2\pi[(\gamma + \gamma_{\rm opt})\cos^2\phi + \gamma\sin^2\phi]} \quad (7)$$

with the maximum for $\phi = 0$. In case (ii), the harmonic approximation of $V(x, y)$ breaks down, and Eq. (6) is evaluated numerically, with the results shown in Figs. 2(d) and 2(e) which are in agreement with the numerical integration of Eq. (5) shown in Fig. 2(b).

In the rigid-rotor regime (iii), motion in the radial direction is suppressed, so that $\sqrt{x^2(t) + y^2(t)} = x_0$ and we can derive a Langevin equation for ϕ alone: $mx_0\ddot{\phi} = -m(\gamma + \gamma_{\rm opt}\cos^2\phi)\dot{\phi} + \xi_\phi$ where $\xi_\phi = \xi_x \sin\phi + \xi_y \cos\phi$ so that $\langle \xi_\phi(t)\xi_\phi(t')\rangle = k_B T m\gamma\delta(t - t')$ is independent of ϕ. This equation describes thermal motion of the orientation of the dimer with angle-dependent damping. Since there is no conservative force, the motion is overdamped, so that $\ddot{\phi} \simeq -\gamma(\phi)\dot{\phi}$, where $\gamma(\phi) = \gamma + \gamma_{\rm opt}\cos^2\phi$, and the Fokker-Planck equation reduces to $\partial P/\partial t = (\partial^2/\partial\phi^2)[(\gamma + \gamma_{\rm opt}\cos^2\phi)^{-1}P]$. The normalized stationary solution is

$$P(\phi) = \frac{\gamma + \gamma_{\rm opt}\cos^2\phi}{2\pi\gamma + \pi\gamma_{\rm opt}} \quad (8)$$

and has a maximum at $\phi = 0$.

This motivates the following intuitive picture: The dominant mechanism in (i) is purely geometrical. Here, the distribution $P(x, y)$ is a Gaussian that is squeezed in the direction of cooling x and, therefore, the most likely orientation is $\phi = 0$. In the rigid-rotor case (iii), in which no orientation-dependent energies are involved,

the anisotropy of the steady-state orientation is due to a purely dynamical effect. In this case, the dimer is dynamically attracted to orientations for which the fluctuations in the angular direction are suppressed. The opposite orientation is reached in the intermediate regime (ii), when a third, purely energetical effect, is dominant. The motion is mostly confined to configurations of constant x, for which the potential energy changes from a double harmonic well at $x = 0$ to a single anharmonic well ($V \propto x^4$) at $x = \pm x_0$. With the average kinetic energy $\langle T \rangle$ constant and using the virial theorem $\langle V \rangle = 2/n\langle T \rangle$, with n the power of the external potential, we find that the probability $\exp[-\beta_x \langle V \rangle]$ is largest for $\phi = \pi/2$.

Let us consider the experimental feasibility in a configuration as shown in Fig. 1. The confinement of the dumbbells to the xy plane can be provided by an external standing wave optical trap crossing the Fabry-Perot cavity in the z direction. The three relevant time scales can be controlled over a large range of parameters: Dimer frequencies up to $\nu \simeq 2\pi \times 1$ kHz can be reached, e.g., with spring constant $k \simeq 0.2$ pN/μm of DNA and silica nanospheres with a radius of $r = 50$ nm (mass $m = 1.2 \times 10^{-18}$ kg). We note that spring constants of orders of magnitude smaller are possible above the persistence length of 50 nm [33]. The optical damping is provided by a cavity with length $L \simeq 10^{-2}$ m and mode waist of $w \simeq 10^{-4}$ m. We find the optomechanical coupling $g \simeq 2\pi \times 10^4$ Hz via the mode volume $C = (\pi/4)Lw^2$. We further assume a cavity finesse of $\mathcal{F} \simeq 10^5$, so that $\kappa \simeq 2 \times 10^5$ Hz at a wavelength of $\lambda = 1064$ nm. When we further choose $\bar{\Delta} \gtrsim 5\kappa$, a power for the cooling laser of $P_{\text{drive}} = 3 \times 10^{-5}$ W results in a cooling rate of $\gamma_{\text{opt}} \lesssim 2\pi \times 4$ Hz. For the thermal environment we assume room temperature $T = 293$ K and $\gamma = 0.05$ Hz, which corresponds for the chosen nanospheres to an air pressure of approximately 10^{-5} mbar. Note that even lower pressures and environmental damping have recently been achieved experimentally for slightly larger silica nanospheres by optical feedback cooling [34].

Many-body phases.—Liquid crystal phases of dimers have been previously studied in equilibrium and nonequilibrium [28]. Nonisotropic friction and the resulting ordering may offer novel tools to guide the self-assembly towards preferred structures and to study novel nematic phases. We numerically study the system described by the Eq. (5) with the experimental parameters as given above. Figure 3(a) depicts an ensemble of dimers without optical friction. For this choice of parameters, the system is in the liquid phase and the dimer orientations are distributed uniformly. Additional nonisotropic cooling with $\gamma_{\text{opt}}/\gamma = 100$ induces a nonequilibrium transition to a phase characterized by the single- and many-dimer order parameters respectively shown in Figs. 3(b) and 3(c). The single dimers are still aligned. In addition, the interplay between orientation and many-body dynamics leads to a remarkable

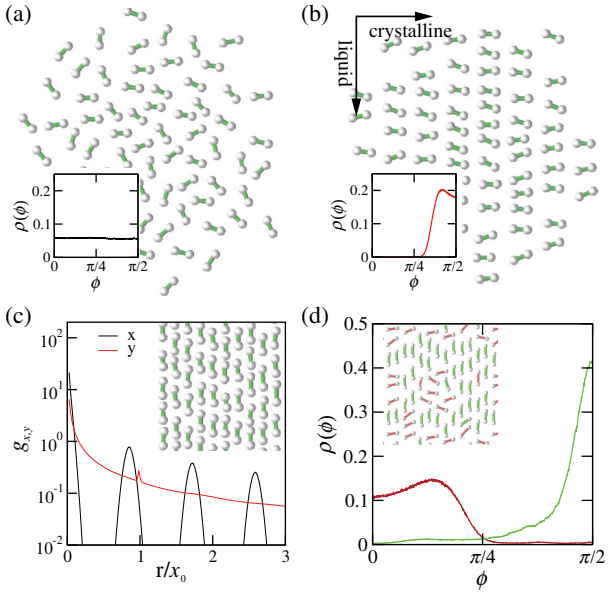

FIG. 3 (color online). (a) Ensemble of dimers with frequency $\nu = 200\gamma$ [intermediate regime (ii)] in thermal equilibrium are uniformly orientated (inset a). (b) The nonisotropic optical friction induces orientational ordering of individual dimers [inset (b)] and in addition, many-body nematic ordering along the direction of cooling. (c) The nonequilibrium phase analog to a liquid crystal phase characterized by the pair-correlation function $g(x)$. The rigid rotors align orthogonal to cooling with additional nematic order in the direction of cooling (black line) and liquid order in the y direction (red line). (d) Mixture of dimers self-assembles into a crystal with dimer-orientations according to the frequencies ν.

phase with liquid order in the y direction and solid order in the x direction. With the frequency $\nu' = 500\nu$ and keeping all other parameters fixed, a different pattern with all individual dimers reorientated orthogonal to the direction of cooling [Fig. 3(c)] is found. Again the many-body dynamics leads to ordering along the x direction, as measured by the directional pair-correlation function $g_{x,y}(x) = \langle \delta((x_i - x_j) - x) \rangle$ depicted in Fig. 3(c). The patterns in Figs. 3(b) and 3(c) are nonequilibrium analogs of liquid crystal phases in equilibrium. For large Γ_0 above the melting temperature [6], two-dimensional dipolar particles self-assemble into a triangular lattice. The guided orientation of individual dimers induced by nonisotropic friction is competing with the orientation in the triangular lattice in which the dimer orientations are random integer multiples of $\pi/3$. This frequency-dependent ordering can be used to create patterns of dimers with different orientations. Figure 3(d) depicts a mixture of dimers with $\nu_1 = 500\nu$ and with $\nu_2 = \nu$. In the absence of direct interactions these species order with almost orthogonal relative alignment. Increasing the interactions $\Gamma_0 > \Gamma_{\text{melt}}$ above the critical melting temperature, the system forms a crystal with triangular ordering and separate orientational order of the two individual dimer species.

In summary, we have presented a realistic optomechanical setup that allows for novel dissipative control over the orientation of dimers composed of nanospheres. We have shown that this approach can be used to prepare nonequilibrium analogs of liquid crystals and to study transitions in mixtures of multiple species of dimers. The only relevant parameters that determine the nonequilibrium ordering are the time scales of the vibrational mode of the dimers and the rates of thermalization and nonisotropic friction. Complex structures of DNA-connected nanospheres are of growing interest, and we hope that the approach discussed here will provide useful means to optical control of such systems, complementary to direct optical manipulation via optical tweezers. The presented mechanism does not rely on any specific properties of nanospheres and applies, at least in principle, in general to complex structures of dielectric objects, such as viruses and bacteria [35]. We speculate that, in the longer run, it may also be applied to complex molecules, and may even prove fruitful as a microseeding technique for the nucleation of complex molecules.

We thank P. Rabl, C. W. Gardiner, M. Grünwald, and C. Dellago for fruitful discussions. Work at Innsbruck is supported by the integrated project AQUTE and by the Institut für Quanten information. Work at Vienna is supported by the integrated project QESSENCE, by an ERC Starting Grant and by a FWF START grant. Both are supported by the Austrian Science Fund through SFB F40 FOQUS.

*w.lechner@uibk.ac.at

[1] K. Dholakia and T. Čižmár, Nat. Photonics **5**, 335 (2011).
[2] A. Ashkin, J. M. Dziedzic, J. E. Bjorkholm, and S. Chu, Opt. Lett. **11**, 288 (1986).
[3] D. G. Grier, Nature (London) **424**, 21 (2003).
[4] V. Prasad, D. Semwogerere, and E. R. Weeks, J. Phys. Condens. Matter **19**, 113102 (2007).
[5] U. Gasser, E. R. Weeks, A. Schofield, P. N. Pusey, and D. A. Weitz, Science **292**, 258 (2001).
[6] C. Eisenmann, U. Gasser, P. Keim, G. Maret, and H.-H. von Grünberg, Phys. Rev. Lett. **95**, 185502 (2005).
[7] T. Bohlein and C. Bechinger, Phys. Rev. Lett. **109**, 058301 (2012).
[8] A. Pertsinidis and X. S. Ling, Phys. Rev. Lett. **87**, 098303 (2001).
[9] D. E. Chang, C. A. Regal, S. B. Papp, D. J. Wilson, J. Ye, O. Painter, H. J. Kimble, and P. Zoller, Proc. Natl. Acad. Sci. U.S.A. **107**, 1005 (2010).
[10] O. Romero-Isart, M. L. Juan, R. Quidant, and J. I. Cirac, New J. Phys. **12**, 033015 (2010).
[11] O. Romero-Isart, A. C. Pflanzer, F. Blaser, R. Kaltenbaek, N. Kiesel, M. Aspelmeyer, and J. I. Cirac, Phys. Rev. Lett. **107**, 020405 (2011).
[12] H. K. Cheung and C. K. Law, Phys. Rev. A **86**, 033807 (2012).
[13] T. Li, S. Kheifets, D. Medellin, and M. G. Raizen, Science **328**, 1627 (2010).
[14] T. J. Kippenberg and K. J. Vahala, Opt. Express **15**, 17 172 (2007).
[15] J. D. Thompson, B. M. Zwickl, A. M. Jayich, F. Marquardt, S. M. Girvin, and J. G. E. Harris, Nature (London) **452**, 72 (2008).
[16] F. Marquardt and S. Girvin, Physics **2**, 40 (2009).
[17] I. Pikovski, M. R. Vanner, M. Aspelmeyer, M. S. Kim, and Č. Brukner, Nat. Phys. **8**, 393 (2012).
[18] P. Meystre, arXiv:1210.3619.
[19] D. Leibfried, R. Blatt, C. Monroe, and D. Wineland, Rev. Mod. Phys. **75**, 281 (2003).
[20] M. T. Woodside, W. M. Behnke-Parks, K. Larizadeh, K. Travers, D. Herschlag, and S. M. Block, Proc. Natl. Acad. Sci. U.S.A. **103**, 6190 (2006).
[21] D. Collin, F. Ritort, C. Jarzynski, S. B. Smith, I. Tinoco, Jr., and C. Bustamante, Nature (London) **437**, 231 (2005).
[22] W. J. Parak, D. Gerion, T. Pellegrino, D. Zanchet, C. Micheel, S. C. Williams, R. Boudreau, M. A. Le Gros, C. A. Larabell, and A. P. Alivisatos, Nanotechnology **14**, R15 (2003).
[23] Y. Wang, Y. Wang, D. R. Breed, V. N. Manoharan, L. Feng, A. D. Hollingsworth, M. Weck, and D. J. Pine, Nature (London) **491**, 51 (2012).
[24] C. M. Niemeyer, Angew. Chem., Int. Ed. Engl. **40**, 4128 (2001).
[25] V. N. Manoharan, M. T. Elsesser, and D. J. Pine, Science **301**, 483 (2003).
[26] A. J. Mastroianni, S. A. Claridge, and A. P. Alivisatos, J. Am. Chem. Soc. **131**, 8455 (2009).
[27] D. Frenkel, H. N. W. Lekkerkerker, and A. Stroobants, Nature (London) **332**, 822 (1988).
[28] R. A. L. Jones, *Soft Condensed Matter* (Oxford University Press, New York, 2006).
[29] P. D. Olmsted and P. Goldbart, Phys. Rev. A **41**, 4578 (1990).
[30] A. F. Demirörs, P. M. Johnson, C. M. van Kats, A. van Blaaderen, and A. Imhof, Langmuir **26**, 14466 (2010).
[31] A. Xuereb, P. Domokos, J. Asbóth, P. Horak, and T. Freegarde, Phys. Rev. A **79**, 053810 (2009).
[32] See Supplemental Material at http://link.aps.org/supplemental/10.1103/PhysRevLett.110.143604 for details of the derivations.
[33] C. Bustamante, S. B. Smith, J. Liphardt, and D. Smith, Curr. Opin. Struct. Biol. **10**, 279 (2000).
[34] J. Gieseler, B. Deutsch, R. Quidant, and L. Novotny, Phys. Rev. Lett. **109**, 103603 (2012).
[35] A. Ashkin and J. M. Dziedzic, Science **235**, 1517 (1987).